RSC Advances

ROYAL SOCIETY OF CHEMISTRY

www.rsc.org/advances

Journal Name

ARTICLE

Rapid Growth of Vertically Aligned Multi-Walled Carbon Nanotubes on a Lamellar Support

Received 00th January 20xx,
Accepted 00th January 20xx

DOI: 10.1039/x0xx00000x

www.rsc.org/

N. M. Briggs[a] and S. P. Crossley*[a]

Vertically aligned carbon nanotubes offer several advantages over nanotubes synthesized using traditional techniques. An inherent disadvantage of vertically aligned nanotubes is the necessary use of low surface area flat catalyst supports during synthesis that are not easily amenable to scale up. Attempts to synthesize nanotubes within layers of a lamellar support in a scalable manner in a fluidized bed while protecting the catalyst surface from attrition have been limited to lower reaction temperatures and slow growth rates due to rapid particle sintering. This article reports on the synthesis of vertically aligned multi-walled carbon nanotube (V-MWNT) forests with heights over 80 µm and growth rates eight times faster than previously reported in a fluidized bed on lamellar supports. The addition of an Al precursor to Fe and Co catalyst precursors between layers of mica clay was found to play a key role in the promotion of nanotube forest growth. The volume expansion in the catalyst after synthesis of the V-MWNTs was correlated to the average nanotube forest length to obtain a simple bulk descriptor of forest height. Modifications to the reduction and reaction temperatures enabled control over the carbon nanotube diameters. Forests with V-MWNT diameters as large as 33 nm and small as 7 nm were obtained, with the smallest diameter V-MWNTs being double and triple walled.

Introduction

Carbon nanotubes have found uses in a variety of applications ranging from catalyst supports to electronic devices.[1-7] The vertical alignment of carbon nanotube forests exhibit several advantages over non-aligned carbon nanotubes that tend to agglomerate. The unique orientation of the carbon nanotubes makes them useful because of their field emission properties[8] and their self-cleaning capabilities resulting from the super hydrophobicity created by the lotus leaf effect of their arrays.[9] Vertically aligned carbon nanotubes have also shown promise for use in thermal management,[10] hydrogen storage,[11, 12] sensors,[13] yarns,[14,15] energy adsorbing hybrid composites,[16] compressible foams,[17] lithium-ion batteries,[5] hydrophobic coatings,[2] oil adsorption,[18] and applications that require strong adhesive forces.[19]

An additional key benefit of vertically aligned carbon nanotubes is the reduced catalyst weight required to produce a given amount of nanotubes as a result of longer lengths. The reduced catalyst requirement could enable the use of carbon nanotubes in applications that would otherwise be cost prohibitive.[20] In addition, due to the unconfined growth in a vertical array, Hata *et al.* reported that the addition of small amounts of water during the synthesis can result in ultra long (up to 2.5 mm) vertically aligned nanotubes in ten minutes.[21] Due to the increased length, a carbon purity of 99.98% was achieved and the carbon nanotubes could more easily be removed from the substrate.[21] This easy separation from the substrate and high purity should eliminate the need for typical purification processes that may create defects[20] and change the point of zero charge of the carbon nanotubes.[22]

The synthesis of aligned carbon nanotubes was first reported on mesoporous silica in 1996[23] and on glass in 1998.[24] Two approaches to further increase the yield of vertical carbon nanotube arrays that have been proposed are by moving flat substrates on a conveyor belt[25,26] and by using lamellar clay supports in fluidized beds.[16,27-30] By synthesizing the nanotubes within the layers of the lamellar support, the vertical growth of the tubes is enabled while avoiding cleavage of the nanotubes from attrition during fluidization. While vertical carbon nanotubes have been grown on substrates with different geometries, including flakes[31], spheres[32-35], and fibers[36], lamellar supports[16,27-30] have shown the best potential to produce the highest ratio of nanotube weight per gram of catalyst.[27] The longest reported vertical carbon nanotubes arrays produced over lamellar supports are 50 µm with a growth rate a rate of 20 µm/h. While these lengths are promising for fluidized bed growth and indicate there is potential to grow longer vertically aligned carbon nanotubes in large quantities, there is significant room for improvement to approach the nanotube lengths obtained on single flat substrates.

In this article, the growth of vertically aligned multi-walled carbon nanotubes (V-MWNTs) is investigated in a fluidized bed using lamellar supports while incorporating alumina within the catalyst to inhibit metal particle sintering. We report V-MWNT growth rates of 160 µm/h with lengths over 80 microns, which is 8 times faster than the highest rate reported over lamellar supports with unprecedented lengths.[16,27-30] Only a small handful of literature reports[16,27-30] investigate V-MWNTs growth with lamellar clay supports. Most literature on lamellar supports reports growth of randomly oriented carbon nanotubes.[37-41] The limited work on this subject only emphasizes the need to further understand these systems to maximize length and production of vertically aligned

[a] 100 East Boyd Street, School of Chemical, Biological, and Materials Engineering, University of Oklahoma, Norman, OK 73071, United States of America. E-mail: stevencrossley@ou.edu

Electronic Supplementary Information (ESI) available: [details of any supplementary information available should be included here]. See DOI: 10.1039/x0xx00000x

carbon nanotube arrays. This article, therefore, reports on the role of varying amounts of Al, Fe, and Co, the method by which the catalyst is deposited, and the effect of reduction and reaction temperatures. The role of elevated catalyst impregnation temperature is also discussed. A typical approach for increasing carbon nanotube length is to increase the reaction temperature, however, this typically results in larger diameter carbon nanotubes.[42,43] This article shows that by modifying the catalyst loading, alumina concentration, reduction temperature, and partial pressure of the carbon source, the length of the V-MWNTs grown between layers of a lamellar catalyst support can be increased with a minimal increase in nanotube diameter. The critical role of an aluminium precursor is also discussed, which inhibits sintering and enables the use of higher temperatures where longer carbon nanotubes and more rapid growth rates are achieved.

Experimental Section

Mica grade V-5 muscovite with a lateral size of 75 mm by 50 mm and thickness of 0.15 mm was purchased from SPI Supplies/Structure Probe, Inc. The mica sheets were then cut into small rectangular pieces roughly 2 mm by 2 mm and placed in a beaker of water. A T25 Digital Ultra Turrax with dispersant element IKA S 25 N – 18 GA was then used to break the mica sheets into small mica flakes by homogenizing them in water for three minutes at 10,000 rpm. The flakes were then sieved to sort out sizes between 150 and 355 µm using Cole Parmer mesh screens.

For wet impregnation of the mica flakes, Iron (III) nitrate nonahydrate, Cobalt (II) nitrate hexahydrate, and Aluminium nitrate nonahydrate were added to a beaker to obtain the desired metal concentrations. Fifty millilitres of either 18 MΩ water or isopropanol (IPA) was then added to the beaker as a solvent and the solution was mixed to dissolve the catalyst precursors. Two grams of the mica flakes were then placed in a mesh boat with a sieve size of 66 µm. The mesh boat was then placed in a glass petri dish and the catalyst solution was poured into the petri dish. The mica flakes were then soaked in the solution for two hours, after which the mesh boat was slowly removed from the solution and hung for two days to allow for excess catalyst solution to drip off and for the catalyst solution to dry.

The mica flakes were then calcined in air in a Thermolyne 48000 furnace for two hours at 450°C. To grow the V-MWNTs, 100 mg of the catalyst was placed on top of a quartz frit in the center of a 1 inch diameter quartz tube. The quartz tube was oriented vertically, so that fluidization of the mica flakes could take place. The catalyst was reduced by increasing the temperature to either 560°C or 650°C at a rate of 10°C per minute under a hydrogen flow rate of 300 sccm. The temperature was then held at the desired reduction temperature for 30 minutes with a hydrogen flow rate of 300 sccm. After reduction, the temperature was increased to the desired reaction temperature at a rate of 10°C per minute at a nitrogen flow rate of 300 sccm. The temperature was then held at the reaction temperature for 10 minutes under nitrogen flow to bring the reactor temperature to a steady state. Ethylene or a mixture of ethylene and nitrogen was then introduced for 30 minutes with a total flow rate of 400 sccm. After the reaction, the reactor was allowed to cool to room temperature under a flow rate of 300 sccm nitrogen.

Table 1 contains the sample labels, precursor concentrations, solvent used to dissolve the catalyst, temperature of reduction and reaction, and flow rates of ethylene and hydrogen used during reaction.

For SEM characterization, a Zeis NEON 40 EsB SEM was used to determine vertical alignment of the V-MWNTs and take images for measurement of their lengths using ImageJ software. For TEM characterization, a JEOL 2010F high resolution TEM, equipped with a field emission gun, was used to take images that were used to measure the diameter distribution of the carbon nanotubes. Measurement of the inner and outer diameters was determined by using ImageJ software. The average inner and outer diameter measurements of 100 randomly selected nanotubes were used to obtain an estimate of the average number of walls assuming an average nanotube wall thickness of 0.344 nm.[44] To test the validity of this method the number of walls for 100 carbon nanotubes were also counted for three samples. The three samples were HRRx760, HRRx650D, and HRRx650D-D, which span a range from an average of 4 to 32 walls. Both methods for determining the number of carbon nanotube walls gave comparable results as can be seen in the Electronic Supplementary Information (ESM). The validity of this approach is further supported by Chiodarelli *et al.*, who came to the same conclusion upon correlating the number of walls of multiwalled carbon nanotubes to their diameters.[45] Carbon yields were determined by oxidizing the carbon nanotubes and catalyst in air to 800°C in the previously described calcination

Table 1 Sample Description. NoAl = No alumina layer made, HW = hot water was used a solvent, W = Water was used as a solvent, D = ethylene was diluted with nitrogen, and HR = reduction temperature of 650°C.

Samples	Metal precursor concentration (mM)			Solvent	Temperature of		Flow rate (sccm)	
	Fe	Co	Al		Reduction (°C)	Reaction (°C)	C_2H_4	N_2
NoAlRx760	2.6	0.7	0	Isopropanol	560	760	400	0
WRx760	2.6	0.7	5.3	Water	560	760	400	0
HWRx760	2.6	0.7	5.3	Water (Heated)	560	760	400	0
Rx760	2.6	0.7	5.3	Isopropanol	560	760	400	0
HRRx760	2.6	0.7	5.3	Isopropanol	650	760	400	0
HRRx650	2.6	0.7	5.3	Isopropanol	650	650	400	0
HRRx650D	2.6	0.7	5.3	Isopropanol	650	650	200	200
HRRx650D-A	2.2	1.1	5.3	Isopropanol	650	650	200	200
HRRx650D-B	2.6	0.7	2.6	Isopropanol	650	650	200	200
HRRx650D-C	2.2	1.1	2.6	Isopropanol	650	650	200	200
HRRx650D-D	2.2	1.1	2.6	Isopropanol	650	700	200	200

system and measuring the resulting weight loss using a Metler Toledo AL204 analytical balance.

Temperature Programmed Reduction (TPR) experiments were conducted by flowing 5% H_2 in Ar at a rate of 30 sccm over a packed bed of 60 mg of mica flakes with catalyst. A temperature increase of 10°C per minute starting at room temperature and ending at 900°C was used. Analysis of effluent gas was detected with an SRI 110 thermal conductivity detector (TCD). The effluent gas was dried by passing through a packed bed filled with Drierite before introduction into the TCD detector.

Results and Discussion

Relationship between volume of nanotube arrays and nanotube length

A noticeable change in the volume of the mica flakes can be observed during the nanotube growth. This can be attributed to the expansion of the mica via V-MWNT growth between the layers. An average length of the V-MWNTs is measured for each sample by estimating the lengths of over 50 arrays via SEM imaging. The volume of the recovered catalyst and nanotubes post reaction are plotted against the average lengths of the V-MWNTs as shown in Figure 1. All reaction data obtained with pure ethylene used during the reaction step is plotted in Figure 1 (a) while the results obtained with an ethylene stream diluted with N_2 during the reaction step are shown in Figure 1 (b). The role of reactant dilution is discussed in following sections of this article. Carbon yield is also plotted versus average V-MWNT length as shown by Figure S1 & S2 of the ESM. These figures show a linear correlation in both cases but the slope is not as pronounced as the volume expansion of the material. As will be discussed in the following sections, a small fraction of the ethylene decomposes during the reaction to form an amorphous carbon layer under certain conditions. This leads to a more direct and pronounced correlation between the catalyst volume expansion and nanotube length when compared to the relationship between volume expansion and carbon yield.

To demonstrate the important role of Al in the growth of V-MWNTs on mica flakes, Fe and Co catalysts were tested without any additional Al precursor. This approach does not create a V-MWNT forest upon reaction at 760°C as shown for sample NoAlRx760 in Figure 2(a) with only small fragments of non aligned carbon nanotubes observed.

Precursors that decompose to form alumina have been shown to play a critical role in the synthesis of V-MWNTs by Fe catalysts supported on silicon wafers.[21,46,47] The incorporation of an Al precursor during catalyst synthesis results in a similar positive influence resulting in the production VMWNT arrays on lamellar supports as shown in Figure 1(a) and 2(b). The increase in both length and volume, shown by comparison of samples NoAlRx760 and Rx760, is significant since the only change is the incorporation

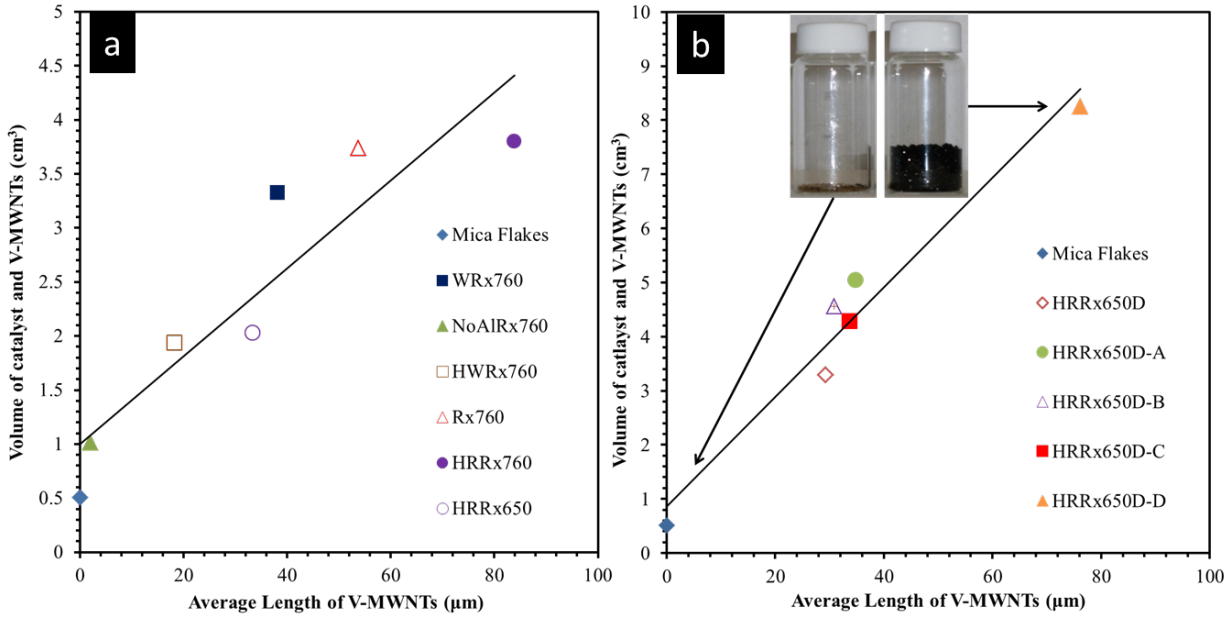

Figure 1 (a) Correlation between volume of catalyst and V-MWNTs and average length of V-MWNTs when only ethylene is used during the reaction step. (b) Correlation between volume of catalyst and V-MWNTs and average length of V-MWNTs when ethylene is diluted with nitrogen during the reaction step.

of an Al precursor with the Fe and Co catalyst. The average V-MWNT length increased from 1 to 50 µm and the volume increased from one cm^3 to almost four cm^3, as can be seen in Figure 1(a). As observed on non-lamellar supports, alumina likely hinders the sintering of the catalyst particles responsible for growth of the carbon nanotubes, as has been shown by Mattevi *et al.*[46] and Kaneko *et al.*[47] Both groups showed reduced sintering of the iron by using alumina resulting in a narrower carbon nanotube diameter because of the narrower catalyst size distribution when compared to silica supported catalysts. This reduction in the rate of sintering is likely responsible for the longer growth of V-MWNTs in a shorter time frame than was achieved by other groups that previously synthesized vertically aligned carbon nanotubes between lamellar supports.[16,27-30]

Mattevi *et al.* showed the existence of Fe^{2+} and Fe^{3+} and their strong interaction with the surface oxygen atoms of the alumina support by using in-situ X-ray photoelectron spectroscopy and annealing under H_2 and Ar at 580°C.[46] This group found, however, that only metallic Fe existed on a silica surface, when annealed under the same conditions. Interface states formed between the Fe

and surface oxygen atoms of the alumina were proposed to help reduce the surface mobility, which are not present when Fe is supported on silica. Because no interfacial states formed between Fe and silica, the Fe coalesces into large islands. It can, therefore, be concluded that the Al precursor is likely forming interface states with the Fe, which is reducing the sintering of Fe and promoting growth of the V-MWNTs. An Al precursor is therefore incorporated in all samples discussed hereafter.

The role of heating the catalyst and mica flakes during impregnation at 80°C in reflux for 24 hours was investigated by preparing a sample, HWRx760, in a similar manner to literature reports.[27, 28, 30] Other studies report catalyst impregnation in lamellar supports at ambient temperatures,[16] with no clear rationale for either impregnation technique. Samples HWRx760, WRx760 and Rx760 serve to elucidate the role of heating solvent choice during wet impregnation of the catalyst within layers of mica flakes. An Al precursor was incorporated in each case.

Previous reports demonstrated growth of V-MWNT arrays between layers of lamellar clay supports of approximately 10 µm in nanotube length in half an hour,[16, 27-30] while sample HWRx760 shows growth of 20 µm over the same period of time. As can be seen in Figure 1(a) for sample HWRx760, the volume expands to approximately two cm^3 post reaction. SEM and TEM results are shown in Figure S3 of the ESM along with outer and inner diameters of the V-MWNTs. During preparation of sample HWRx760, the heating turned the catalyst solution from a transparent orange to a dark red color. The darker color of the heated solution could be due to the formation of insoluble iron hydroxide particulates, in agreement with literature observations.[48]

By maintaining the catalyst solution at ambient temperature the formation of the precipitate is avoided, with the resulting catalyst sample designated as WRx760. V-MWNT length significantly increased over the heated precursor impregnation sample, HWRx760, as can be seen in Figure 1(a). This result implies that insoluble iron hydroxide particulates hinder V-MWNT growth. SEM and TEM images can be seen in Figure S4 of the ESM, along with inner and outer diameter measurements of the V-MWNTs.

To test the impact of the solvent during catalyst impregnation, isopropanol was used as a solvent in place of water, sample Rx760. Replacing isopropanol with water as a solvent yielded an increase in V-MWNT length as shown in Figure 2(b), and volume of material as shown in Figure 1(a). Measurements of the V-MWNTs from TEM images, such as Figure 2(c), indicate their average outer and inner diameters to be 19.2±6.9 nm and 6.7±2.3 nm, respectively, and with an average wall number of 18. The variance in growth resulting from the two different solvents during catalyst deposition may due to (i) hindered amounts of iron hydroxide formation in isopropanol or (ii) isopropanol, having a lower surface tension th water, may have created a more uniform coating of catalyst upon evaporation of the solvent. The lower surface tension may have resulted in the catalyst being left behind as the isopropanol

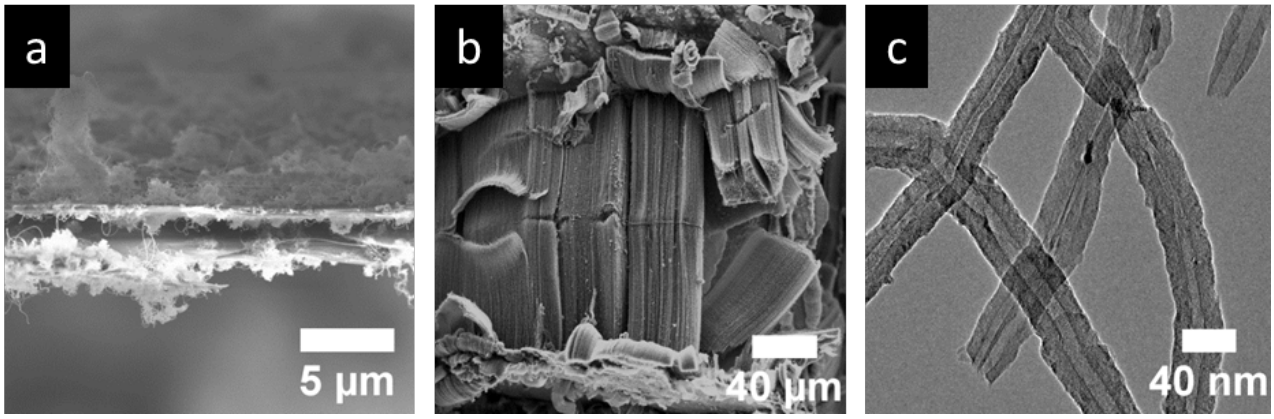

Figure 2 (a) SEM image of sample NoAlRx760 without incorporation of alumina, (b) SEM image of sample Rx760, incorporation of alumina, and (c) TEM image of sample Rx760.

evaporated whereas with water a higher surface tension will pull the catalyst particles to the remaining liquid as evaporation occurs. Isopropanol appears to be a superior catalyst deposition solvent, and as will be discussed in the following sections, further optimization of reaction conditions using this deposition technique results in V-MWNT lengths over 80 µm and a volume expansion of almost four cm^3.

During the reaction step when pure ethylene was flowed above 700°C, an orange-yellow colored gas was produced due to pyrolysis of ethylene. The quartz glass tube after reaction was coated with a black opaque layer of carbon. Similar observations have been reported during V-MWNT growth with ethylene in the literature.[34] It is possible this pyrolysis of ethylene is producing carbon that is coking and deactivating catalyst particles or possibly fusing layers of the mica.

To overcome the problem of fast coking or fusing layers of mica together, ethylene was diluted with nitrogen during the reaction step. The dilution of the ethylene resulted in a large increase in V-MWNTs volume and a decrease in diameter as shown in Figure 1(b), which will be discussed in later sections. This indicates there is more growth of V-MWNT arrays since the detrimental impact of high ethylene concentrations is minimized. Regardless of whether nitrogen was or was not used to dilute the ethylene during the reaction step, a linear relationship was found between the average length of the V-MWNTs and the volume of the samples post reaction as shown in Figure 1(b).

Role of reduction temperature

V-MWNTs with lengths over 80 µm were obtained for sample HRRx760 by increasing the reduction temperature to 650°C. Inner and outer diameters of the V-MWNTs of sample HRRx760 were 8.3±1.9 nm and 32±3.5 nm respectively, resulting in an average number of 36 walls per nanotube. SEM and TEM images of sample HRRx760 can be seen in the supplementary information, Figure S5

of the ESM. A reasonable explanation for the increased length of the V-MWNTs is that the Fe and Co have been reduced to a greater extent at 650°C, as shown by the TPR in Figure 3.

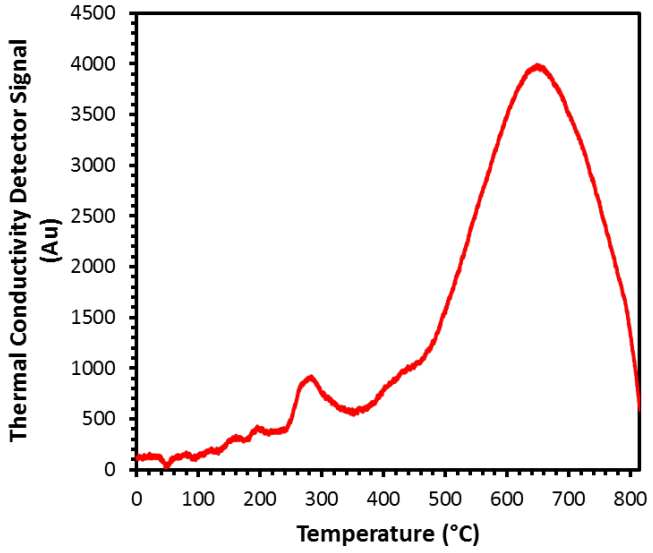

Figure 3 Temperature programmed reduction of catalyst used for samples RX760, HRRX760, HRRX650, and HRRX650D.

When the Fe and Co is not fully reduced, the ethylene serves as the reducing agent, potentially at the expense of excessive carbon deposition, that may deactivate the catalyst for V-MWNTs growth.

Consistent with Brown *et al.* the major reduction of bulk Fe and Co is around 650°C, see Figure 3.[49] The peak at 300°C shown on Figure 3 was observed by this group for both Fe and Co. Brown *et al.* attributed this peak to well dispersed Fe and Co on the alumina. The maximum hydrogen uptake was found to be greater at lower temperatures as the Co to Fe ratio increased, which is observed in the TPR profile shown in Figure S6 of the ESM. Mossbauer spectroscopy revealed as the Co to Fe ratio increased Fe and Co spinels formed because of the depletion of Fe_2O_3 by Co.[50] The role of the Co to Fe ratio on V-MWNT growth will be discussed in the following sections.

Growth of few walled V-MWNTs

Due to the assumption that excessive pyrolysis occurs when flowing pure ethylene, the ethylene was diluted with nitrogen and the reaction temperature lowered for this research in an attempt to decrease the diameter of the V-MWNTs and to produce few-walled V-MWNTs, defined as two to five layers of side walls and diameters between three to eight nm.[51] To study the effect of diluting the ethylene and lowering the reaction temperatures both cases were studied, using increased reduction temperature of 650°C instead of 560°C. Sample HRRx650 is the result of lowering the reaction temperature, which resulted in no observable pyrolysis or oil coating the glass reactor vessel during the reaction step. Based on SEM and TEM images Figure S7 of the ESM, V-MWNT lengths up to 30 µm were produced with average outer and inner diameters of 6.9±2.4 nm and 3.7±1.3 nm, respectively. From this information, the average number of V-MWNT walls was determined to be five, with some double and triple walled V-MWNTs present.

Carbon nanotube yield can be increased by changing the partial pressure of the carbon source.[52] To increase the yield of V-MWNTs, the partial pressure of ethylene was modified while keeping all other parameters the same as for sample HRRx650. To change the partial pressure of ethylene, an equal volume of nitrogen and ethylene were flown, sample HRRx650D. This ratio of ethylene to nitrogen results in an increase in volume expansion with the same catalyst, Figure 1 (a & b). The V-MWNTs produced are up to 30 µm in length as shown in Figure 4 (a).

An explanation for the increase in volume of the collected material is the change in partial pressure, which decreased the amount of catalyst particles that were deactivated or inaccessible due to the excessive ethylene partial pressures. TEM results for sample HRRx650D are similar to results shown for sample HRRx650. Sample HRRx650 shows an average V-MWNT outer diameter of 6.8±2.4 nm and inner diameter of 3.9±2.4 nm, and an average of 4 walls with some double and triple walls being present as shown in Figure 4 (b). The use of the proper reduction temperature allows for a lower reaction temperature to be used and still grow longer V-MWNTs with few walls. Dilution of the ethylene during the reaction step increased the yield of V-MWNTs.

Role of catalyst ratios and temperature

The role of the Co to Fe ratio was modified in an attempt to increase the length of the V-MWNTs without increasing the

Journal Name

ARTICLE

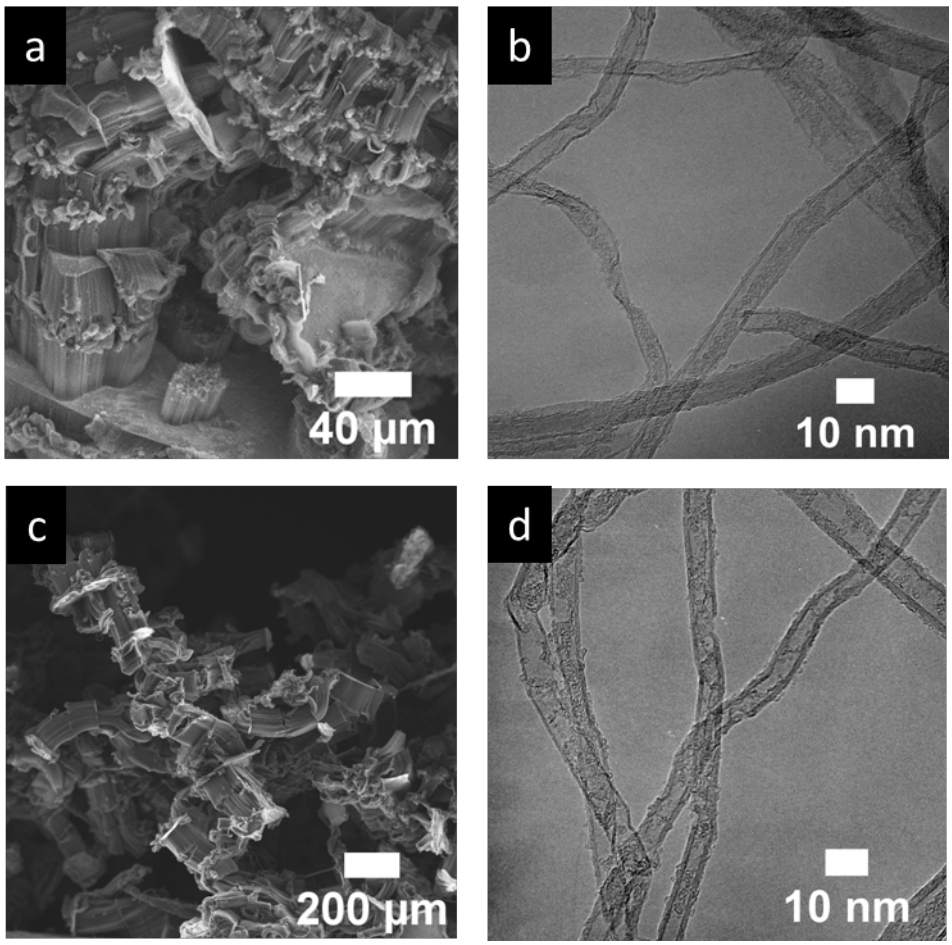

Figure 4 (a) SEM image of sample HRRx650D, decrease in partial pressure of ethylene and reduction temperature of 650°C (b) TEM image of sample HRRx650D, (c) SEM image of sample HRRx650D-D, reaction temperature of 700°C and catalyst precursor of Al decreased and Co increased, and (d) TEM image of sample HRRx650D-D.

V-MWNTs' diameters, which is usually the case when increasing temperature.[42, 43] The synergistic effect of Fe and Co has been shown to give a higher yield of carbon nanotubes than either Fe or Co alone.[53] Increasing the Co to Fe ratio for sample HRRx650D-A, resulted in an increase in V-MWNT length and volume compared to using a lower Co to Fe ratio as used for sample HRRx650D. TEM results show that the average diameter and number of walls for sample HRRx650D-A are comparable to HRRx650D. SEM and TEM images for sample HRRx650D-A are in Figure S8 of the ESM. Two possible reasons for the increased length and volume expansion of material are, (i), the Co helps to reduce the Fe further[48] and, (ii) the formation of Fe and Co spinels may hinder particle sintering.[49]

Excessive amounts of the Al precursor could possibly coat the Fe and Co and render them inactive. The role of Al precursor concentration was explored by decreasing the concentration by half as shown for sample HRRx650D-B. With the reaction conditions kept the same as for sample HRRx650D, there was an increase in the volume of V-MWNTs and the mica. TEM results indicate that the average diameters and the number of walls were similar to samples HRRx650D-A and HRRx650D. SEM and TEM images can be found in the Figure S9 of the ESM. By decreasing the amount of Al precursor, more Fe and Co may be exposed for growing V-MWNTs, which is a likely reason for the increased volume expansion.

While improvements in the volume expansion and length of the V-MWNTs are observed by either increasing the amount of Co or decreasing the amount of Al in the sample, further improvements are not obtained by combining both strategies. HRRx650D-C was prepared with both a higher Co and lower Al loading. This resulted in an effect similar to both samples HRRx650D-B and HRRx650D-C, in which neither a significant volume expansion or length change of the V-MWNTs occurred. TEM results for sample HRRx650D-C show no significant change in average diameter or number of walls. Supplementary information has SEM

and TEM images of sample HRRx650D-C as shown by Figure S10 of the ESM.

The reaction temperature has a significant influence on the final nanotube length and diameter. This is illustrated by sample HRRx650D-D, which was prepared using the same catalyst as in sample HRRx650D-C at a higher reaction temperature of 700°C. The results of these changes are quite dramatic showing a significant increase in the length of the V-MWNTs, over 80 µm, and a significant volume expansion in material as shown in Figure 4(c). The V-MWNTs grew at a rate of 160 µm/h, which is eight times faster than previously reported.[16, 27-30] In addition to the length and significant volume expansion, the diameter of the V-MWNTs doubled to an average outer diameter of 11.5±3.5 nm, average inner diameter of 5.6±1.8 nm, and average wall number of 9, as shown in Figure 4(d). Increased nanotube diameters as a function of temperature have also been reported in the literature using vermiculite clay supports.[30] The increase in growth of the V-MWNT arrays results in the separation of layers within the mica sheets, as can be seen in Figure 4(c). This finding is in agreement with those reported by Zhang *et al.* who observed unequal rates of nanotube growth along the mica surfaces resulting in fracturing of the mica sheets.[27]

Conclusions

The synthesis of V-MWNTs in a scalable fashion over lamellar supports at lengths greater than those reported in the literature is achieved. This is accomplished through the incorporation of Co and Al within the Fe catalyst to promote metal reduction and reduce sintering. Few walled V-MWNTs with lengths of up to 40 µm are synthesized via this approach. The incorporation of Al enables increased growth temperatures, resulting in V-MWNTs over 80 µm in length. The height of the expanded mica flakes post reaction shows a linear correlation with the average MWNT length. Modifications in precursor concentration, catalyst deposition method, and reaction temperature allow for control of both nanotube length and diameter in lamellar supports.

Acknowledgements

This work was supported by U.S. Department of Energy, DOE/EPSCOR (Grant DESC0004600). We acknowledge Alexander Schwans for help with the reactions, Greg Strout for his help with transmission electron microscopy, and Preston Larson for his help with scanning electron microscopy.

Notes and references

1. S. Crossley, J. Faria, M. Shen, and D. E. Resasco, *Science*, 2010, **327**, 68-72.
2. K. K. Lau, J. Bico, K. B. Teo, M. Chhowalla, G. A. Amaratunga, W. I. Milne, G. H. McKinley, and K. K. Gleason, *Nano letters,* 2003**, 3**, 1701-1705.
3. H. Wang and E. K. Hobbie, *Langmuir*, 2003**, 19**, 3091-3093.
4. W. Chen, X. Liu, Y. Liu, Y. Bang and H. I. Kim, *Journal of Industrial and Engineering Chemistry,* 2011*,* **17**, 455-460.
5. D. T. Welna, L. Qu, B. E. Taylor, L. Dai, and M. F. Durstock, *Journal of Power Sources*, 2011**, 196**, 1455-1460.
6. A. Star, V. Joshi, S. Skarupo, D. Thomas, and J. C. P. Gabriel, *The Journal of Physical Chemistry B*, 2006**, 110**, 21014-21020.
7. A. Javey, J. Guo, D. B. Farmer, Q. Wang, D. Wang, R. G. Gordon, M. Lundstrom, and H. Dai, *Nano Letters*, 2004, **4**, 447-450.
8. S. Fan, M. G. Chapline, N. R. Franklin, T. W. Tombler, A. Cassell, and H. Dai, *Science*, 1999, **283**, 512-514.
9. I. Y. Bu and S. P. Oei, *Applied surface science*, 2010, **256**, 6699-6704.
10. W. Lin, R. Zhang, K. S. Moon, and C. P. Wong, *Advanced Packaging, IEEE Transactions on*, 2010**, 33**, 370-376.
11. A. Cao, H. Zhu, X. Zhang, X. Li, D. Ruan, C. Xu, B. Wei, J. Liang, and D. Wu, *Chemical physics letters*, 2001, **342**, 510-514.
12. H. Zhu, A. Cao, X. Li, C. Xu, Z. Mao, D. Ruan, J. Liang, and D. Wu, *Applied surface science*, 2001, **178**, 1, 50-55.
13. J. Yang, R. Zhang, Y. Xu, P. He, and Y. Fang, *Electrochemistry Communications*, 2008, **10**, 1889-1892.
14. K. Jiang, Q. Li, and S. Fan, *Nature*, 2002, **419**, 801-801.
15. M. Zhang, K. R. Atkinson, and R. H. Baughman, *Science*, 2004, **306**, 1358-1361.
16. Q. Zhang, M. Zhao, Y. Liu, A. Cao, W. Qian, Y. Lu, and F. Wei, *Advanced Materials*, 2009, **21**, 2876-2880.
17. A. Cao, P. L. Dickrell, W. G. Sawyer, M. N. Ghasemi-Nejhad, and P. M. Ajayan, *Science*, 2005**, 310**, 1307-1310.
18. M. Q. Zhao, J. Q. Huang, Q. Zhang, W. L. Luo, and F. Wei, *Applied Clay Science*, 2011, **53**, 1-7.
19. L. Qu, L. Dai, M. Stone, Z. Xia, and Z. L. Wang, *Science*, 2008, **322**, 238-242.
20. C. M. Seah, S. P. Chai, and A. R. Mohamed, *Carbon*, 2011, **49**, 4613-4635.
21. K. Hata, D. N. Futaba, K. Mizuno, T. Namai, M. Yumura, and S. Iijima, *Science*, 2004, **306**, 1362-1364.
22. O. Matarredona, H. Rhoads, Z. Li, J.H. Harwell, L. Balzano, and D. E. Resasco, *The Journal of Physical Chemistry B*, 2003**, 107**, 13357-13367.
23. W. Z. Li, S. S. Xie, L. Qian, B. H. Chang, B. S. Zou, W. Y. Zhou, A. Zhao, and G. Wang, *Science*, 1996, **274**, 1701-1703.
24. Z. F. Ren, Z. P. Huang, J. W. Xu, J. H. Wang, P. Bush, M. P. Siegal, and P. N. Provencio, *Science*, 1998, **282**, 1105-1107.
25. R. G. de Villoria, S. L. Figueredo, A. J. Hart, S. A. Steiner III, A. H. Slocum, and B. L. Wardle, *Nanotechnology*, 2009, **20**, 405611.
26. R. Guzmán de Villoria, A. J. Hart, and B. L. Wardle, *ACS nano*, 2011, **5**, 4850-4857.
27. Q. Zhang, M. Q. Zhao, J. Q. Huang, Y. Liu, Y. Wang, W. Qian, and F. Wei, *Carbon*, 2009, **47**, 2600-2610.
28. Q. Zhang, M. Q. Zhao, J. Q. Huang, and F. Wei, *Powder Technology*, 2010, **198**, 285-291.
29. M. Q. Zhao, Q. Zhang, J. Q. Huang, and F. Wei, *Journal of Physics and Chemistry of Solids*, 2010, **71**, 624-626.
30. Q. Zhang, M. Q. Zhao, J. Q. Huang, J. Q. Nie, and F. Wei, *Carbon*, 2010, **48**, 1196-1209.
31. C. L. Pint, S. T. Pheasant, M. Pasquali, K. E. Coulter, H. K. Schmidt, and R. H. Hauge, *Nano letters*, 2008, **8**, 1879-1883.

32. R. Xiang, G. H. Luo, W. Z. Qian, Y. Wang, F. Wei, and Q. Li, *Chemical Vapor Deposition*, 2007, **13**, 533-536.
33. R. Xiang, G. Luo, Z. Yang, Q. Zhang, W. Qian, and F. Wei, *Materials Letters*, 2009, **63**, 84-87.
34. Q. Zhang, J. Q. Huang, M. Q. Zhao, W. Z. Qian, Y. Wang, and F. Wei, *Carbon*, 2008, **46**, 1152-1158.
35. R. Philippe, B. Caussat, A. Falqui, Y. Kihn, P. Kalck, S. Bordère, D. Plee, P. Gaillard, D.Bernard, and P. Serp, *Journal of Catalysis*, 2009, **263**, 345-358.
36. F. An, C. Lu, J. Guo, S. He, H. Lu, and Y. Yang, *Applied Surface Science*, 2011, **258**, 1069-1076.
37. A. Bakandritsos, A. Simopoulos, and D. Petridis, *Chemistry of materials*, 2005, **17**, 3468-3474.
38. D. Manikandan, R. V. Mangalaraja, R. E. Avila, R. Siddheswaran, and S. Ananthakumar, *Materials Science and Engineering: B*, 2012, **177**, 614-618.
39. D. Manikandan, R. V. Mangalaraja, R. E. Avila, R. Siddheswaran, and S. Anathakumar, *Applied Clay Science*, 2013, **71**, 37-41.
40. F. C. Moura and R. M. Lago, *Applied Catalysis B: Environmental*, 2009, **90**, 436-440.
41. A. D. Purceno, B. R. Barrioni, A. Dias, G. M. da Costa, R. Lago, and F. C. Moura, *Applied Clay Science*, 2011, **54**, 15-19.
42. Y. Huh, J. Y. Lee, J. Cheon, Y. K. Hong, J. Y. Koo, T. J. Lee, and C. J. Lee, *Journal of Materials Chemistry*, 2003, **13**, 2297-2300.
43. N. S. Kim, Y. T. Lee, J. Park, J. B. Han, Y. S. Choi, S. Y. Choi, J. Choo, and G. H. Lee, *The Journal of Physical Chemistry B*, 2003, **107**, 9249-9255.
44. Y. Saito, T. Yoshikawa, S. Bandow, M. Tomita, and T. Hayashi, *Physical Review B*, 1993, **48**, 1907.
45. N. Chiodarelli, O. Richard, H. Bender, M. Heyns, S. D. Gendt, G. Groeseneken, P. M. Vereecken, *Carbon*, 2012, **50**, 1748-1752.
46. C. Mattevi, C. T. Wirth, S. Hofmann, R. Blume, M. Cantoro, C. Ducati, C. Cepek, A. Knop-Cericke, S. Milne, C. Castellarin-Cudia, S. Dolafi, A. Goldoni, R. Schloegl, and J. Robertson, *The Journal of Physical Chemistry C*, 2008, **112**, 12207-12213.
47. A. Kaneko, K. Yamada, R. Kumahara, H. Kato, and Y. Homma, *The Journal of Physical Chemistry C*, 2012, **116**, 26060-26065.
48. H. R. Barzegar, F. Nitze, T. Sharifi, M. Ramstedt, C. W. Tai, A. Malolepszy, L. Stobinski, and T. Wågberg, *The Journal of Physical Chemistry C*, 2012, **116**, 12232-12239.
49. R. Brown, M. E. Cooper, and D. A. Whan, *Applied Catalysis*, 1982, **3**, 177-186.
50. M. J. Tricker, P. P. Vaishnava, and D. A. Whan, *Applied Catalysis*, 1982, **3**, 283-295.
51. Y. Hou, J. Tang, H. Zhang, C. Qian, Y. Feng, and J. Liu, *ACS nano*, 2009, **3**, 1057-1062.
52. J. E. Brown, M.S. Dissertation, University of Oklahoma, 2011.
53. N. Nagaraju, A. Fonseca, Z. Konya, and J. B. Nagy, *Journal of Molecular Catalysis A: Chemical*, 2002, **181**, 57-62.